frontiers in Materials

ORIGINAL RESEARCH
published: 07 August 2020
doi: 10.3389/fmats.2020.00216

# Hydrothermal Synthesis of Flake-Flower NiO and Its Gas Sensing Performance to CO

*Guochao Qian[1,2]*, Qingjun Peng[1], Dexu Zou[1], Shan Wang[1] and Bing Yan[1]*

*[1] Electric Power Science Research Institute of Yunnan Power Grid Co., Ltd., Kunming, China, [2] State Key Laboratory of Power Transmission Equipment & System Security and New Technology, Chongqing University, Chongqing, China*

In this work, flake-flower NiO was successfully prepared via a facile hydrothermal method. The microstructure of the synthesized sample was characterized by X-ray powder diffraction (XRD), scanning electron microscopy (SEM), and transmission electron microscopy (TEM). We find that the hierarchical flake-flower structure was assembled by numerous nanosheets with different size and shape. The fabricated sensor based on the obtained microstructure exhibited excellent gas sensing performance including high response, outstanding selectivity and stability toward 5 ppm CO at the optimal working temperature of 250°C. A plausible gas sensing mechanism was given out to explain how the nanosheet assembly morphology affects the gas sensing performance of the flake-flower structure.

**Keywords: hydrothermal, NiO, flake-flower, gas sensor, CO**

OPEN ACCESS

***Edited by:***
*Kezhen Qi,*
*Shenyang Normal University, China*

***Reviewed by:***
*Matteo Tonezzer,*
*Italian National Research Council, Italy*
*S. V. Prabhakar Vattikuti,*
*Yeungnam University, South Korea*

****Correspondence:***
*Guochao Qian*
*164688847@qq.com*

***Specialty section:***
*This article was submitted to Thin Solid Films, a section of the journal Frontiers in Materials*

***Received:*** *13 May 2020*
***Accepted:*** *12 June 2020*
***Published:*** *07 August 2020*

***Citation:***
*Qian G, Peng Q, Zou D, Wang S and Yan B (2020) Hydrothermal Synthesis of Flake-Flower NiO and Its Gas Sensing Performance to CO. Front. Mater. 7:216. doi: 10.3389/fmats.2020.00216*

## INTRODUCTION

Dissolved Gas in Oil Analysis (DGA) is one of the most convenient and effective methods to judge the early latent faults of oil immersed high-voltage electrical equipment at present (Gui et al., 2019; Yang et al., 2019a; Zhou et al., 2019; Wang et al., 2020; Wei et al., 2020a). As one of the most important fault characteristic gases of oil immersed transformer, carbon monoxide (CO), has received considerable attention for its application to provide vital help for judging the operation state of transformer (Zhou et al., 2015, 2018a,b; Yang et al., 2019b). In this respect, to detect and analyze the dissolved gases, many strategies have been proposed, for instance, gas chromatography, photoacoustic spectrometry and gas sensor (Qu et al., 2016; Liu et al., 2017; Wei et al., 2019b). Among these methods, the design of gas sensor has attracted numerous interest, owing to its low cost, facile route and simple structure (Wang et al., 2019a; Zargouni et al., 2019). However, to ensure the normal operation of transformer and power system, the fabrication of high-performance gas sensors is still a still a challenging work (Wei et al., 2019c; Zhou et al., 2018c; Zhang et al., 2019).

In order to fabricate high-performance gas sensors among various metal oxide semiconductors, which includes ZnO (Zhou et al., 2013; Zhu et al., 2017, 2018a), $SnO_2$ (Zhang et al., 2014, 2017; Ahmed et al., 2019), $WO_3$ (Park et al., 2014; Du et al., 2018; Li et al., 2018), $TiO_2$ (Zeng et al., 2012; Zhang Y. X. et al., 2018), and NiO (Zhang H. et al., 2018; Zhou et al., 2018d; Devarayapalli et al., 2019), Nickel oxide (NiO) has gained increasing attention for its wide band gap energy (3.6–4.0 eV) and stable physical and chemical properties (Sun et al., 2016; Zhang Y. et al., 2016; Wang et al., 2017; Nagajyothi et al., 2019). Besides, a lot of studies have confirmed that NiO is a promising nanomaterial to detect the fault characteristic gas in transformer oil (Dang et al., 2015; Li et al., 2015; Beroual and Haddad, 2017).

Considering that the morphology of the nanomaterials plays an important role in the gas sensing performance of NiO sensors, there have been considerable efforts in the synthesis of different NiO nanostructures for instance nanoparticle (0-D) (Cao et al., 2016; Kruefu et al., 2016), nanorod (1-D) (Choi et al., 2016; Feng et al., 2017), nanosheet (2-D) (Yu et al., 2015; Sta et al., 2016) and nanoflower (3-D) (Wang et al., 2016; Miao et al., 2017). Compared with low dimensional nanostructures, hierarchical nanostructures have made great progress because of their complicated and beneficial structures (Cao et al., 2015; Wang et al., 2015). For example, Wei et al. (2019a) designed and synthesized 2-D NiO porous nanosheet via a facile hydrothermal method, the gas sensor based on which had excellent gas sensing performance toward 30 ppm $H_2$ at the optimal working temperature of 225°C benefited from the special porous nanostructure. Wang et al. (2019b) synthesized hierarchical structure assembled with NiO nanosheets and the sensor based on the nanostructure exhibited excellent gas sensing performance due to its high special surface area. Reasonable design of hierarchical structure of NiO is a challenging but meaningful work to enhance the performance of NiO based sensor to detect the fault characteristic gas in transformer oil (Zhang D. Z. et al., 2016; Balamurugan et al., 2017; Cui et al., 2019).

In this work, hierarchical flake-flower NiO has been prepared with a facile hydrothermal method. The obtained sample was characterized by XRD, SEM, TEM, HRTEM, and SAED and fabricated into gas sensing device. Gas sensing test toward CO was carried out to demonstrate the high-performance of the special hierarchical NiO structure. The gas sensing results indicated that the fabricated sensor showed excellent performances including high response, prominent stability and outstanding selectivity toward 5 ppm CO at the optimal working temperature of 250°C. A plausible gas sensing mechanism was proposed, demonstrating that the excellent performance might be caused by the hierarchical 3-D structure with high special surface area.

# EXPERIMENTAL

## Synthesis of Flake-Flower NiO

All reagents in this work used to prepare the hierarchical flake-flower NiO were of analytical grade and used without any further purification. In a typical hydrothermal procedure, 0.475 g $NiCl_2{\cdot}6H_2O$ was added into 20 ml mixed solution composed of 10 ml of pure water and 10 ml of ethanol. Then, 0.2 g PVP and 10 ml of EG were added into the mixture under stirring. The pH value of the solution was adjusted to about 10 by dropping $NH_3{\cdot}H_2O$. After that, the mixture was magnetically stirred for 5 min to form a homogeneous solution and then poured into a 50 mL Teflon-lined stainless autoclave which was kept at 140°C for 10 h. After the autoclave cooled to room temperature, the green sample was harvested by centrifugation and washing with pure water and ethanol for several times. After drying at 60°C for 10 h, the expected product was obtained by calcination at 600°C for 1 h.

## Materials Characterization

The structure and phase purity of the product were characterized by X-ray diffraction (XRD) with a Rigaku D/Max-2550 diffractometry (Cu-Kα radiation, $\lambda$ = 0.15418 nm, $2\theta$ = 30–85°). The morphology of the flake-flower NiO was observed by a Nova 400 scanning electronic microscope (SEM). The high-magnification structure of the flake-flower morphology was investigated by a JEM-2100F field-emission transmission electron microscope including transmission electron microscope (TEM), high resolution transmission electron microscope (HRTEM) and selected area electron diffraction (SAED).

## Gas Sensor Measurements

In order to fabricate high-performance CO sensing sensor based on the flake-flower NiO, the device was designed with a side-heated structure as shown in **Figure 1A**. Concretely, the prepared sample was mixed with pure water and ethanol in a ratio of 8:1:1 to obtain a homogeneous solution which was used to form a

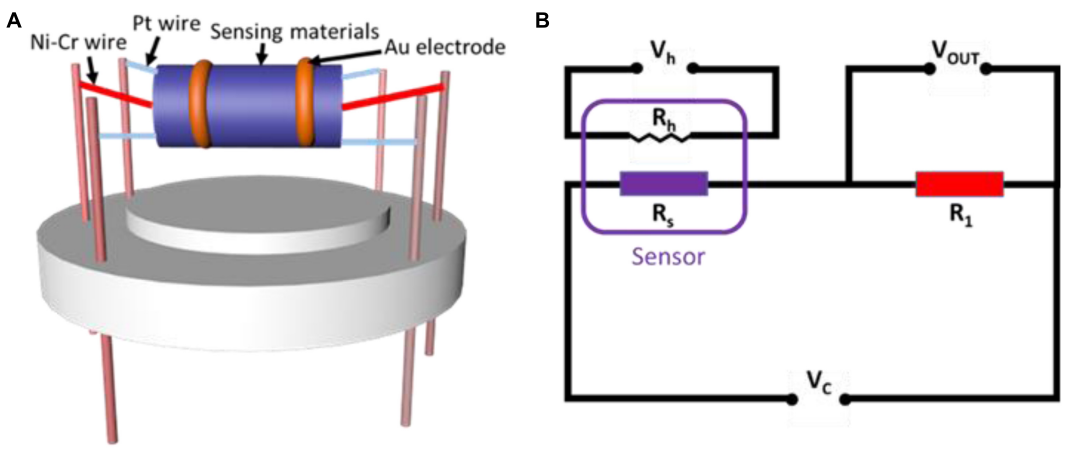


**FIGURE 1 | (A)** Schematic structure of the gas sensor. **(B)** The measuring electric circuit of the sensor.

sensing film. Then, the formed film was coated onto a ceramic tube which has been designed with a pair of Au electrodes and two pairs of Pt wires. Next, a Ni-Cr wire was inserted into the tube to control the working temperature of the sensor (Zhang et al., 2015; Zhu et al., 2018b). **Figure 1B** gives out the theoretic diagram of the test circuit, from which one can find that $V_{out}$ represents the output voltage to calculate the resistance and $V_h$ represents

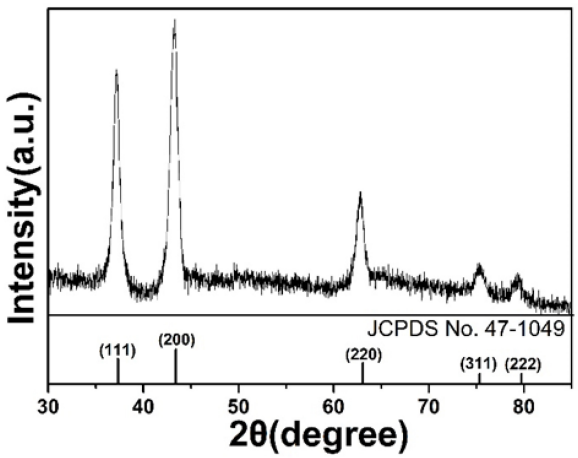


**FIGURE 2 |** XRD patterns of the prepared sample.

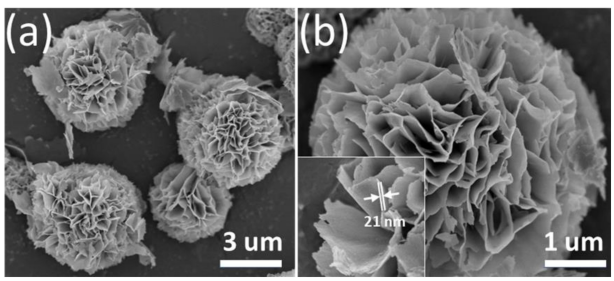


**FIGURE 3 |** SEM images of the flake-flower microstructure at low **(a)** and corresponding high **(b)** magnification.

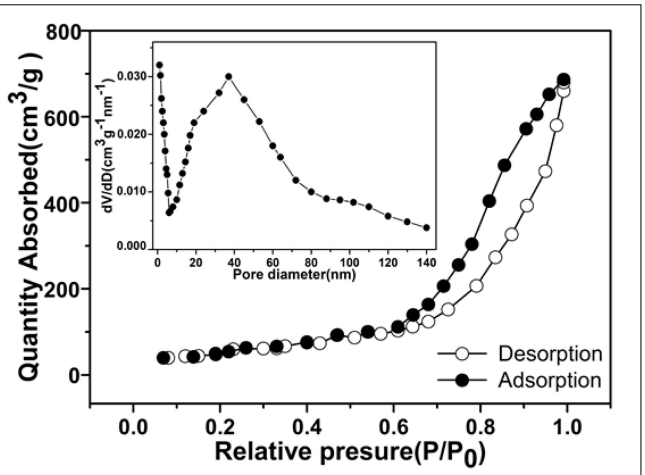


**FIGURE 5 |** Typical nitrogen adsorption-desorption isotherms and BJH pore size distribution analysis.

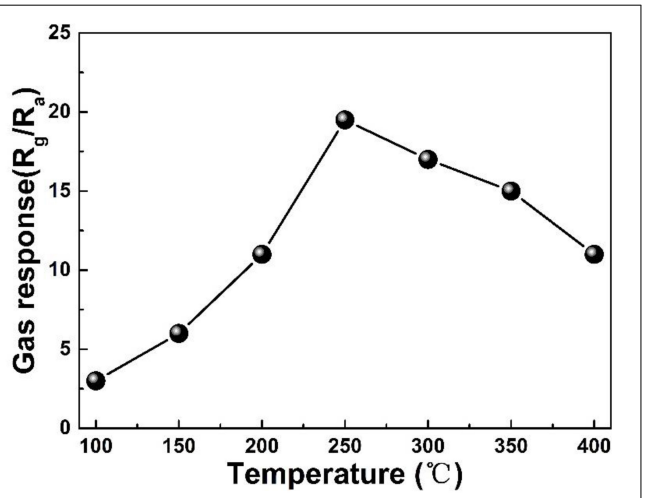


**FIGURE 6 |** Gas responses of flake-flower NiO based gas sensor toward 5 ppm CO at different temperature from 100 to 400°C.

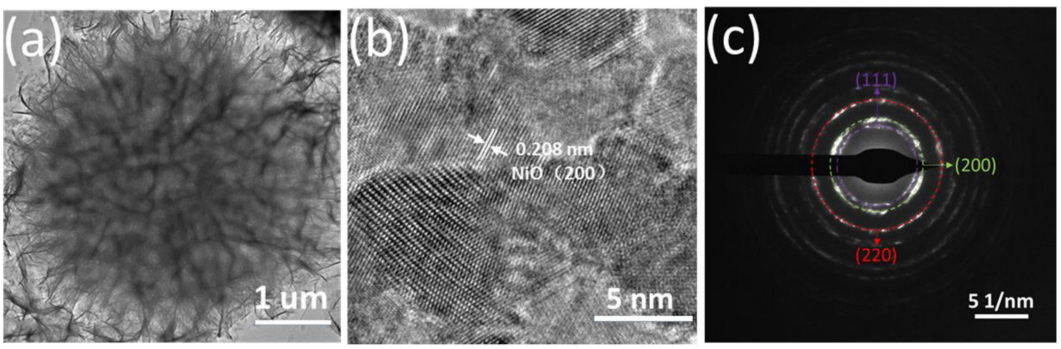


**FIGURE 4 | (a)** TEM image of NiO; **(b)** HRTEM image of NiO; **(c)** SAED pattern of NiO.

the heating voltage to change the working temperature (Wei et al., 2019b). To ensure the long-term stability and repeatability of the fabricated CO sensor, the device was aged at 300°C for 1 week in air (Lu et al., 2018). The gas sensing performance of the fabricated sensor was measured with a static analysis system using a Chemical Gas Sensor-8 intelligent system (Beijing Elite Tech Co., Ltd.). Besides, the volume of the test chamber is 20 L and the flux of the test gases was set to 20 ml/min. Gas response in this work were defined as $S = R_g/R_a$, in which $R_g$ and $R_a$ represent the resistances in target gases and in air (Wei et al., 2020b).

## RESULTS AND DISCUSSION

### Morphology and Structure

The structure and phase purity of the synthesized flake-flower sample were characterized by XRD as shown in **Figure 2**. From the XRD pattern, it is obvious that there are five clear diffraction peaks at 37.1°, 43.3°, 63.1°, 75.1°, and 79.5°, which can be will indexed with (1 1 1), (2 0 0), (2 2 0), (3 1 1), and (2 2 2) lattice planes of cubic NiO (JCPDS Card no. 47-1049). Besides, no other diffraction peaks were observed in the spectrum, indicating that the prepared product must be pristine NiO with high-purity.

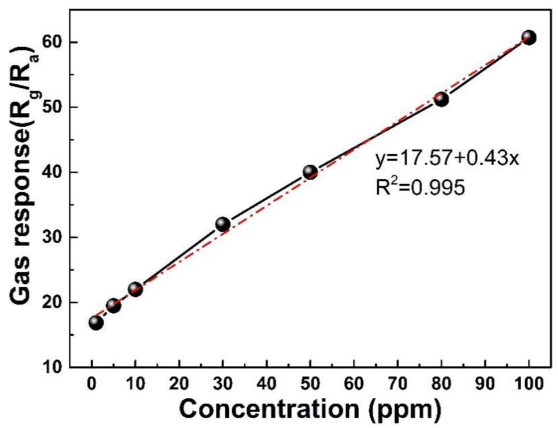


**FIGURE 7 |** Gas responses of flake-flower NiO based gas sensor toward different concentration of CO from 1 to 100 ppm at the optimal working temperature of 250°C.

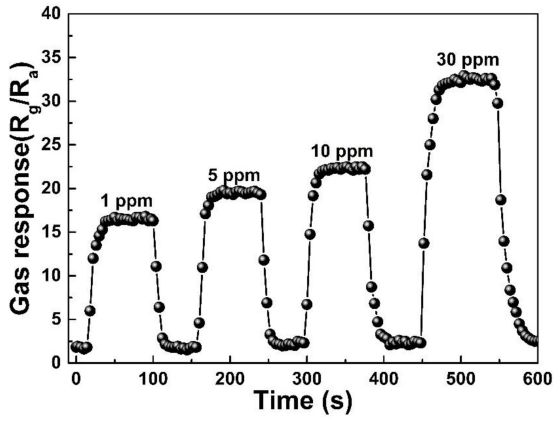


**FIGURE 8 |** The dynamic response-recovery characteristic of the flake-flower NiO based gas sensor toward different concentration of CO (1, 5, 10, 30 ppm) at 250°C.

**Figure 3** displays the SEM micrographs of the flake-flower NiO with different magnification. As shown in **Figure 3a**, it can be seen that the synthesized sample have a flower-like microstructure a relatively uniform distribution and a diameter of about 5 μm. From the higher magnification image of the flower-like microstructure (**Figure 3b**), it is intuitive that the flake-flower structure was assembled by a lot of thin nanosheets. The numerous nanosheets with different shape and size make the NiO structure exhibit a flake-flower shape and hierarchy which will possess large surface sites and abundant reaction rooms for gas molecules.

To observe a more detailed structural information of the flake-flower microstructure, the sample was analyzed by transmission electron microscope with the characterization of TEM, HRTEM and SAED (**Figure 4**). As presented in **Figure 4a**, the structure was confirmed to be assembled by numerous irregular and random nanosheets which have been mentioned in **Figure 3b**. A clear HRTEM image of NiO is displayed in **Figure 4b**, demonstrating the existence of crystalline NiO. From the clear lattice stripes, the lattice spacing can be calculated to be 0.208 nm which corresponded to the (200) plane of the cubic NiO. Moreover, **Figure 4c** depicts the SAED image of synthesized NiO sample, from which one can observe that there are a group of diffraction rings, namely (1 1 1), (2 0 0), and (2 2 0) lattice planes of cubic NiO. To confirm the potential impact of the specific surface area on gas sensing properties, the typical nitrogen adsorption-desorption isotherm was calculated. The BET analysis (**Figure 5**) indicated that the specific surface area of the synthesized flake-flower NiO is 176.5 $m^2g^{-1}$ and the average pore size is 27.6 nm, suggesting that the flake-flower microstructure provided a large surface area.

### Gas Sensing Performance

As we all know, the working temperature of gas sensor has a great influence on the reaction in the process of gas sensing. To obtain the optimal working temperature of the fabricated CO sensor based on the flake-flower NiO, the device was tested at different temperatures from 100 to 400°C toward 5 ppm CO. It can be seen from **Figure 6** that the response of the flake-flower NiO based sensor toward CO of 5 ppm increased first and then decreased with the increase of temperature, suggesting that the response of the sensor is strongly dependent on the working temperature. This is because the low activation energy at low temperature is not enough to support the gas reaction, and the increased temperature will lead to the higher desorption rate. Given this, the gas response will reach a maximum at a specific temperature, which is the optimum working temperature. In this work, the optimum working temperature of the CO sensor is 250°C, at which the highest response is 19.5. And subsequent gas sensing experiments will be carried out at this optimal operating temperature.

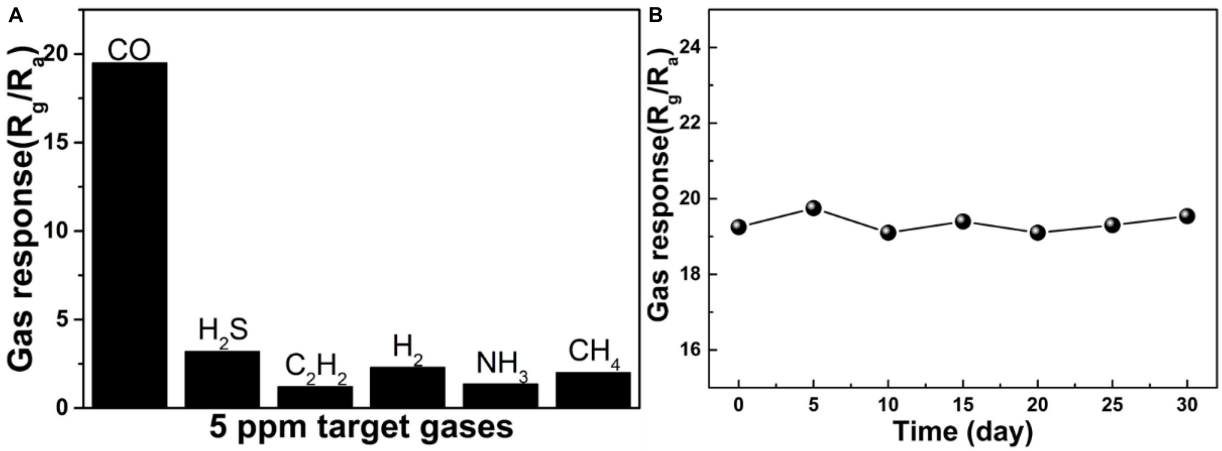


**FIGURE 9 | (A)** The selectivity of the flake-flower NiO based gas sensor toward different 5 ppm gases at 250°C. **(B)** The stability of the flake-flower NiO based gas sensor toward 5 ppm CO for 1 month.

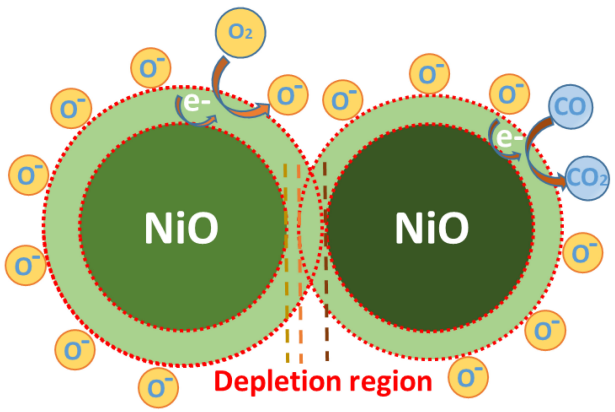


**FIGURE 10 |** The schematic diagram of sensing mechanism.

**Figure 7** presents the response of the flake-flower NiO based sensor toward different concentration of CO at the optimal working temperature of 250°C. Obviously, the response of the fabricated sensor increased almost linearly with the increase of the concentration of CO from 1 to 100 ppm. Besides, the linear fitting function and the linear correlation coefficient were calculated as y = 17.57 + 0.43x and 0.995, respectively. It can be found that the responses of flake-flower NiO based sensor increased obviously linearly with the increasing CO from 1 to 100 ppm at the optimal working temperature of 250°C.

**Figure 8** demonstrates the response and recovery characteristic of the prepared sensor with different concentrations of CO (1, 5, 10, 30 ppm) at the optimal working temperature of 250°C. It is obvious the gas response curve of the sensor increases sharply when CO in, while the gas response curve of the sensor quickly returns to the original state when CO out. The CO responses of the sensor were tested to be 16.9, 19.5, 22.8, and 32.7 under 1, 5, 10, and 30 ppm, respectively. The dynamic response-recovery result indicated that the fabricated sensor possessed excellent reversibility which is an important property for the application of gas sensors.

Considering that selectivity and stability are two important indexes to evaluate the performance of gas sensors, further gas sensing experiments were carried out based on the gas concentration of 5 ppm and the optimal working temperature of 250°C. As shown in **Figure 9A**, the sensor based on the

**TABLE 1 |** Summary of recent researches on NiO based sensors for sensing of toward different reducing gases.

| Sensing material | Gas | Concentration (ppm) | Temp. (°C) | Response | References |
|---|---|---|---|---|---|
| NiO nanowires | $H_2$ | 1000 | 400 | 100% | Hoa et al., 2018 |
| NiO nanowires | $H_2$ | 1000 | 250 | 106.9% | Tonezzer et al., 2017 |
| NiO nanofibers | CO | 10 | 300 | 1.78 | Choi et al., 2016 |
| NiO nanowires | $H_2$ | 1000 | 250 | 107% | Tonezzer et al., 2016 |
| Hollow NiO hemisphere | $C_2H_5OH$ | 200 | 300 | 5 | Cho et al., 2011 |
| NiO nanoparticles | CO | 100 | 350 | 90 | Aslani et al., 2011 |
| Porous NiO microspheres | $H_2S$ | 20 | 200 | 27.2 | Trung et al., 2019 |
| NiO nanoplates | CO | 10 | 275 | 16.39 | Wang et al., 2019b |
| NiO nanosheet | $H_2$ | 30 | 225 | 20.47 | Wei et al., 2019a |
| Flake-flower NiO | CO | 30 | 250 | 32.7 | This work |

flake-flower NiO was exposed toward hydrogen sulfide ($H_2S$), acetylene ($C_2H_2$), hydrogen ($H_2$), ammonia ($NH_3$), methane ($CH_4$), and CO. It can be calculated that the response toward CO is at least 6 times higher than that of other gas, indicating that the NiO based sensor has good selectivity for 5 ppm CO at the optimal working temperature of 250°C, and can be applied for the effective detection of CO. The long-term stability experiment of fabricated CO sensor was carried out for 1 month. The performance of the sensor toward 5 ppm CO at 250°C was tested every 5 day. **Figure 9B** confirms that the prepared device possessed outstanding stability with slight change for 1 month, suggesting the fabricated sensor could be a promising choice for the application to the effective detection of CO.

## Sensing Mechanism

As we all know, the basic gas sensing mechanism is demonstrated by the resistance change caused by the reaction between the adsorbed oxygen molecules and the measured gas molecules. Before injecting the CO gases, the oxygen molecules in the air were adsorbed on the surface of the NiO material due to its strong electronegativity (Cao et al., 2015; Chen et al., 2018, 2019). The oxygen molecules captured the electrons from the surface of NiO material and then were reduced to oxygen ions ($O^-$). For a typical p-type oxide, since the main carrier of NiO is hole, the electrons captured by oxygen mainly come from valence band. This process results in the formation of a hole aggregation layer on the surface of the material, which has a lower resistance compared with the core region (**Figure 10**). The oxygen adsorption mechanism can be expressed as follows:

$$O_{2(g)} \rightarrow O_{2(ads)} \tag{1}$$

$$O_{2(ads)} + 2e^- \rightarrow 2O^-_{(ads)} \tag{2}$$

When the reducing gas CO is introduced, it will react with the oxygen ion adsorbed on the NiO surface to produce $CO_2$ and release electrons at the same time. This process make the released electrons combine with the holes, leading to the increase of the resistance compared with previous state. The process can be described as follows:

$$CO_{(gas)} \rightarrow CO_{(ads)} \tag{3}$$

$$CO_{(ads)} + O^-_{(ads)} \rightarrow CO_2 + e^- \tag{4}$$

Besides, for typical p-type NiO based sensing materials, various strategies have been used to synthesize different nanostructures for the detection of various reducing gases. The gas sensing characteristics of the NiO based sensors of the recently published investigations were listed in **Table 1**, from which we can find that various NiO based sensors possessed excellent gas sensing performances toward different reducing gases.

# CONCLUSION

To summarize, hierarchical flake-flower NiO was successfully synthesized via a facile hydrothermal method. The prepared sample was tested by various structural and morphological characterization, demonstrating that the flake-flower microstructure was assembled by numerous nanosheets with different shape and size. Further CO sensing experiments indicated that the sensor based on the flake-flower NiO exhibited excellent gas sensing performance including high response, outstanding selectivity and stability. A plausible mechanism suggested that the excellent performance was caused by the flake-flower morphology with complicated microstructure and large special surface area. Therefore, the results suggested that flake-flower NiO based CO sensor might be considered as a promising candidate for detecting the fault characteristic gases dissolved in transformer oil.

# DATA AVAILABILITY STATEMENT

The raw data supporting the conclusions of this article will be made available by the authors, without undue reservation, to any qualified researcher.

# AUTHOR CONTRIBUTIONS

All authors listed have made a substantial, direct and intellectual contribution to the work, and approved it for publication.

# REFERENCES


Ahmed, A., Siddique, M. N., Ali, T., and Tripathi, P. (2019). Defect assisted improved room temperature ferromagnetism in Ce doped SnO2 nanoparticles. *Appl. Surf. Sci.* 483, 463–471. doi: 10.1016/j.apsusc.2019.03.209

Aslani, A., Oroojpour, V., and Fallahi, M. (2011). Sonochemical synthesis, size controlling and gas sensing properties of NiO nanoparticles. *Appl. Surf. Sci.* 257, 4056–4061. doi: 10.1016/j.apsusc.2010.11.174

Balamurugan, C., Jeong, Y. J., and Lee, D. W. (2017). Enhanced H2S sensing performance of a p-type semiconducting PdO-NiO nanoscale heteromixture. *Appl. Surf. Sci.* 420, 638–650. doi: 10.1016/j.apsusc.2017.05.166

Beroual, A., and Haddad, A. (2017). Recent advances in the quest for a new insulation gas with a low impact on the environment to replace sulfur hexafluoride (SF6) gas in high-voltage power network applications. *Energies* 10:1216. doi: 10.3390/en10081216

Cao, J., Zhang, H. M., and Yan, X. Q. (2016). Facile fabrication and enhanced formaldehyde gas sensing properties of nanoparticles-assembled chain-like NiO architectures. *Mater. Lett.* 185, 40–42. doi: 10.1016/j.matlet.2016.08.099

Cao, S. K., Zeng, W., Long, H. W., and Zhang, H. (2015). Hydrothermal synthesis of novel flower-needle NiO architectures: structure, growth and gas response. *Mater. Lett.* 159, 385–388. doi: 10.1016/j.matlet.2015.07.045

Chen, K. W., Tsai, J. H., and Chen, C. H. (2019). NiO functionalized Co3O4 hetero-nanocomposites with a novel apple-like architecture for CO gas sensing applications. *Mater. Lett.* 255:126508. doi: 10.1016/j.matlet.2019.126508

Chen, Y., Qin, H., and Hu, J. (2018). CO sensing properties and mechanism of Pd doped SnO2 thick-films. *Appl. Surf. Sci.* 428, 207–217. doi: 10.1016/j.apsusc.2017.08.205

Cho, N. G., Hwang, I. S., Kim, H. G., Lee, J. H., and Kim, I. D. (2011). Gas sensing properties of p-type hollow NiO hemispheres prepared by polymeric colloidal

templating method. *Sens. Actuators B: Chem.* 155, 366–371. doi: 10.1016/j.snb.2010.12.031

Choi, J. M., Byun, J. H., and Kim, S. S. (2016). Influence of grain size on gas-sensing properties of chemiresistive p-type NiO nanofibers. *Sens. Actuators B: Chem.* 227, 149–156. doi: 10.1016/j.snb.2015.12.014

Cui, H., Zhang, X. X., Zhang, G. Z., and Tang, J. (2019). Pd-doped MoS2 monolayer: a promising candidate for DGA in transformer oil based on DFT method. *Appl. Surf. Sci.* 470, 1035–1042. doi: 10.1016/j.apsusc.2018.11.230

Dang, T. T. L., Tonezzer, M., and Nguyen, V. H. (2015). Hydrothermal Growth and Hydrogen Selective Sensing of Nickel Oxide Nanowires. *J. Nanomater.* 2015:785856. doi: 10.1155/2015/785856

Devarayapalli, K. C., Vattikuti, S. V. P., Sreekanth, T. V. M., Yoo, K. S., Nagajyothi, P. C., and Shim, J. (2019). Facile synthesis of Ni-MOF using microwave irradiation method and application in the photocatalytic degradation. *Mater. Res. Express* 6:1150h3. doi: 10.1088/2053-1591/ab5261

Du, Q., Wang, L., Yang, J., Liu, J. F., Yuan, Y. K., Wang, M. Z., et al. (2018). Enhancing gas sensing performances and sensing mechanism at atomic and molecule level of WO3 nanoparticles by hydrogenation. *Sens. Actuators B: Chem.* 273, 1786–1793. doi: 10.1016/j.snb.2018.07.099

Feng, C. B., Kou, X. Y., Chen, B., Qian, G. B., Sun, Y. F., and Lu, G. Y. (2017). One-pot synthesis of In doped NiO nanofibers and their gas sensing properties. *Sens. Actuators B: Chem.* 253, 584–591. doi: 10.1016/j.snb.2017.06.115

Gui, Y. G., Li, T., He, X., Ding, Z. Y., and Yang, P. G. (2019). Pt cluster modified h-BN for gas sensing and adsorption of dissolved gases in transformer oil: a Density Functional Theory Study. *Nanomaterials* 9:1746. doi: 10.3390/nano9121746

Hoa, N. D., Tong, P. V., Hung, C. M., Duy, N. V., and Hieu, N. V. (2018). Urea mediated synthesis of Ni(OH)(2) nanowires and their conversion into NiO nanostructure for hydrogen gas-sensing application. *Int. J. Hydrogen Energ.* 43, 9446–9453. doi: 10.1016/j.ijhydene.2018.03.166

Kruefu, V., Wisitsoraat, A., Phokharatkul, D., Tuantranont, A., and Phanichphant, S. (2016). Enhancement of p-type gas-sensing performances of NiO nanoparticles prepared by precipitation with RuO2 impregnation. *Sens. Actuators B: Chem.* 236, 466–473. doi: 10.1016/j.snb.2016.06.028

Li, F., Ruan, S. P., Zhang, N., Yin, Y. Y., Guo, S. J., Chen, Y., et al. (2018). Synthesis and characterization of Cr-doped WO3 nanofibers for conductometric sensors with high xylene sensitivity. *Sens. Actuators B: Chem.* 265, 355–364. doi: 10.1016/j.snb.2018.03.054

Li, G. H., Wang, X. W., Liu, L., Liu, R., Shen, F. P., Cui, Z., et al. (2015). Controllable Synthesis of 3D Ni(OH)(2) and NiO Nanowalls on Various Substrates for High-Performance Nanosensors. *Small* 11, 731–739. doi: 10.1002/smll.201400830

Liu, H. C., Zhou, Q., Zhang, Q. Y., Hong, C. X., Xu, L. N., Jin, L. F., et al. (2017). Synthesis, characterization and enhanced sensing properties of a NiO/ZnO p-n junctions sensor for the SF6 decomposition byproducts SO2, SO2F2, and SOF2. *Sensors* 17:913. doi: 10.3390/s17040913

Lu, Z., Zhou, Q., Xu, L., Gui, Y., Zhao, Z., Tang, C., et al. (2018). Synthesis and characterization of highly sensitive hydrogen (H2) sensing device based on Ag doped SnO2 nanospheres. *Materials* 11:492. doi: 10.3390/ma11040492

Miao, R. Y., Zeng, W., and Gao, Q. (2017). Hydrothermal synthesis of novel NiO nanoflowers assisted with CTAB and SDS respectively and their gas-sensing properties. *Mater. Lett.* 186, 175–177. doi: 10.1016/j.matlet.2016.09.127

Nagajyothi, P. C., Deyarayapalli, K. C., Tettey, C. O., Vattikuti, S. V. P., and Shim, J. (2019). Eco-friendly green synthesis: catalytic activity of nickel hydroxide nanoparticles. *Mater. Res. Express* 6: 055036. doi: 10.1088/2053-1591/ab04e4

Park, S., Park, S., Jung, J., Hong, T., Lee, S., Kim, H. W., et al. (2014). H2S gas sensing properties of CuO-functionalized WO3 nanowires. *Ceram. Int.* 40, 11051–11056. doi: 10.1016/j.ceramint.2014.03.120

Qu, Z., Fu, Y., Yu, B., Deng, P., Xing, L., and Xue, X. (2016). High and fast H2S response of NiO/ZnO nanowire nanogenerator as a self-powered gas sensor. *Sensor. Actuat. B-Chem.* 222, 78–86. doi: 10.1016/j.snb.2015.08.058

Sta, I., Jlassi, M., Kandyla, M., Hajji, M., Koralli, P., Krout, F., et al. (2016). Surfacefunctionalization of solegel grown NiO thin films with palladium nanoparticles for hydrogen sensing. *Int. J. Hydrogen Energ.* 41, 3291–3298. doi: 10.1016/j.ijhydene.2015.12.109

Sun, G.-J., Kheel, H., Lee, J. K., Choi, S., Lee, S., and Lee, C. (2016). H2S gas sensing properties of Fe2O3 nanoparticle-decorated NiO nanoplate sensors. *Surf. Coat. Tech.* 307, 1088–1095. doi: 10.1016/j.surfcoat.2016.06.066

Tonezzer, M., Le, D. T. T., Huy, T. Q., and Iannotta, S. (2016). Dual-selective hydrogen and ethanol sensor for steam reforming systems. *Sensor. Actuat. B-Chem.* 236, 1011–1019. doi: 10.1016/j.snb.2016.04.150

Tonezzer, M., Le, D. T. T., Tran, Q. H., Nguyen, V. H., and Iannotta, S. (2017). Selective hydrogen sensor for liquefied petroleum gas steam reforming fuel cell systems. *Int. J. Hydrogen Energ.* 42, 740–748. doi: 10.1016/j.ijhydene.2016.11.102

Trung, D. D., Cuong, N. D., Quang, P. L., Anh, N. T. N., Quang, D. T., Nam, P. C., et al. (2019). Facile post-synthesis and gas sensing properties of highly porous NiO microspheres. *Sens. Actuators A: Phys.* 296, 110–120. doi: 10.1016/j.sna.2019.07.014

Wang, C., Liu, J. Y., Yang, Q. Y., Sun, P., Gao, Y., Liu, F. M., et al. (2015). Ultrasensitive and low detection limit of acetone gas sensor based on W-doped NiO hierarchical nanostructure. *Sens. Actuators B: Chem.* 220, 59–67. doi: 10.1016/j.snb.2015.05.037

Wang, C., Zeng, W., and Chen, T. (2017). Facile synthesis of thin nanosheet assembled flower-like NiO-ZnO composite and its ethanol-sensing performance. *J. Mater. Sci-Mater El.* 28, 222–227. doi: 10.1007/s10854-016-5514-1

Wang, J., Zeng, W., and Wang, Z. C. (2016). Assembly of 2D nanosheets into 3D flower-like NiO: synthesis and the influence of petal thickness on gas-sensing properties. *Ceram. Int.* 42, 4567–4573. doi: 10.1016/j.ceramint.2015.11.150

Wang, J. X., Zhou, Q., Lu, Z. R., Wei, Z. J., and Zeng, W. (2019a). Gas sensing performances and mechanism at atomic level of Au-MoS2 microspheres. *Appl. Surf. Sci.* 490, 124–136. doi: 10.1016/j.apsusc.2019.06.075

Wang, J. X., Zhou, Q., Lu, Z. R., Wei, Z. J., and Zeng, W. (2019b). The novel 2D honeycomb-like NiO nanoplates assembled by nanosheet arrays with excellent gas sensing performance. *Mater. Lett.* 255:126523. doi: 10.1016/j.matlet.2019.126523

Wang, J. X., Zhou, Q., Xu, L. N., Gao, X., and Zeng, W. (2020). Gas sensing mechanism of dissolved gases in transformer oil on Ag-MoS2 monolayer: a DFT study. *Physica E* 118:113947. doi: 10.1016/j.physe.2019.113947

Wei, Z. J., Zhou, Q., Wang, J. X., Gui, Y. G., and Zeng, W. (2019a). A novel porous NiO nanosheet and its H2 sensing performance. *Mater. Lett.* 245, 166–169. doi: 10.1016/j.matlet.2019.03.013

Wei, Z. J., Zhou, Q., Wang, J. X., Lu, Z. R., Xu, L. N., and Zeng, W. (2019b). Hydrothermal synthesis of SnO2 nanoneedle-anchored NiO microsphere and its gas sensing performances. *Nanomaterials* 9:1015. doi: 10.3390/nano9071015

Wei, Z. J., Zhou, Q., Lu, Z. R., Xu, L. N., Gui, Y. G., and Tang, C. (2019c). Morphology controllable synthesis of hierarchical WO3 nanostructures and C2H2 sensing properties. *Physica E* 109, 253–260. doi: 10.1016/j.physe.2019.01.006

Wei, Z. J., Zhou, Q., and Zeng, W. (2020a). Hierarchical WO3-NiO microflower for high sensitivity detection of SF6(decomposition)byproduct H2S. *Nanotechnology* 31:215701. doi: 10.1088/1361-6528/ab73bd

Wei, Z. J., Zhou, Q., Wang, J. X., and Zeng, W. (2020b). Hydrothermal synthesis of hierarchical WO3/NiO porous microsphere with enhanced gas sensing performances. *Mater. Lett.* 264:127383. doi: 10.1016/j.matlet.2020.127383

Yang, Z., Zhou, Q., Wu, X. D., Zhao, Z. Y., Tang, C., and Chen, W. G. (2019a). Detection of water content in transformer oil using multi frequency ultrasonic with PCA-GA-BPNN. *Energies* 12:1379. doi: 10.3390/en12071379

Yang, Z., Zhou, Q., Wu, X. D., and Zhao, Z. Y. (2019b). A novel measuring method of interfacial tension of transformer oil combined PSO optimized SVM and multi frequency ultrasonic technology. *IEEE Access* 7, 182624–182631. doi: 10.1109/ACCESS.2019.2954899

Yu, F., Xu, X. L., Peng, H. G., Yu, H. J., Dai, Y. F., Liu, W. M., et al. (2015). Porous NiO nano-sheet as an active and stable catalyst for CH4 deep oxidation. *App. Catal. A* 507, 109–118. doi: 10.1016/j.apcata.2015.09.023

Zargouni, S., Derbali, L., Ouadhour, M., Rigon, M., Martucci, A., and Ezzaouia, H. (2019). Elaboration and characterization of PVP-assisted NiO thin films for enhanced sensitivity toward H2 and NO2 gases. *Ceram. Int.* 45, 5779–5787. doi: 10.1016/j.ceramint.2018.12.044

Zeng, W., Liu, T. M., and Wang, Z. C. (2012). Enhanced gas sensing properties by SnO2 nanosphere functionalized TiO2 nanobelts. *J. Mater. Chem.* 22, 3544–3548. doi: 10.1039/c2jm15017d

Zhang, H., Zeng, W., Zhang, Y., Li, Y. Q., Miao, B., Chen, W. G., et al. (2014). Synthesis and gas sensing properties of novel SnO2 nanorods. *J. Mater. Sci-Mater. El.* 25, 5006–5012. doi: 10.1007/s10854-014-2264-9

Zhang, Q. Y., Zhou, Q., Yin, X. T., Liu, H. C., Xu, L. N., Tan, W. M., et al. (2017). The effect of PMMA pore-forming on hydrogen sensing properties of porous SnO2 thick film sensor. *Sci. Adv. Mater.* 9, 1350–1355. doi: 10.1166/sam.2017.3111

Zhang, W. L., Zeng, W., Miao, B., and Wang, Z. C. (2015). Effect of the sheet thickness of hierarchical SnO2 on the gas sensing performance. *Appl. Surf. Sci.* 355, 631–637. doi: 10.1016/j.apsusc.2015.07.149

Zhang, X. X., Fang, R. X., Chen, D. C., and Zhang, G. Z. (2019). Using Pd-doped gamma-graphyne to detect dissolved gases in transformer oil: a density functional theory investigation. *Nanomaterials* 9:1490. doi: 10.3390/nano9101490

Zhang, Y., Wang, J., Wei, H., Hao, J., Mu, J., Cao, P., et al. (2016). Hydrothermal synthesis of hierarchical mesoporous NiO nanourchins and their supercapacitor application. *Mater. Lett.* 162, 67–70. doi: 10.1016/j.matlet.2015.09.123

Zhang, D. Z., Chang, H. Y., Li, P., and Liu, R. (2016). Characterization of nickel oxide decorated-reduced graphene oxide nanocomposite and its sensing properties toward methane gas detection. *J. Mater. Sci-Mater. El.* 27, 3723–3730. doi: 10.1007/s10854-015-4214-6

Zhang, Y. X., Zeng, W., Ye, H., and Li, Y. Q. (2018). Enhanced carbon monoxide sensing properties of TiO2 with exposed (001) facet: a combined first-principle and experimental study. *Appl. Surf. Sci.* 442, 507–516. doi: 10.1016/j.apsusc.2018.02.036

Zhang, H., Chen, W. G., Li, Y. Q., Jin, L. F., Cui, F., and Song, Z. H. (2018). 3D Flower-like NiO hierarchical structures assembled with size-controllable 1D blocking units: gas sensing performances towards acetylene. *Front. Chem.* 6:472. doi: 10.3389/fchem.2018.00472

Zhou, Q., Chen, W. G., Xu, L. N., and Peng, S. D. (2013). Hydrothermal synthesis of various hierarchical ZnO nanostructures and their methane sensing properties. *Sensors* 13, 6171–6182. doi: 10.3390/s130506171

Zhou, Q., Tang, C., Zhu, S. P., and Chen, W. G. (2015). NiO doped SnO2 p-n heterojunction microspheres: preparation, characterisation and CO sensing properties. *Mater. Technol.* 30, 349–355. doi: 10.1179/1753555715y.0000000010

Zhou, Q., Chen, W. G., Xu, L. N., Kumar, R., Gui, Y. G., Zhao, Z. Y., et al. (2018a). Highly sensitive carbon monoxide (CO) gas sensors based on Ni and Zn doped SnO2 nanomaterials. *Ceram. Inter.* 44, 4392–4399. doi: 10.1016/j.ceramint.2017.12.038

Zhou, Q., Lu, Z. R., Wei, Z. J., Xu, L. N., Gui, Y. G., and Chen, W. G. (2018b). Hydrothermal synthesis of hierarchical ultrathin NiO nanoflakes for high-performance CH4 sensing. *Front. Chem.* 6:194. doi: 10.3389/fchem.2018.00194

Zhou, Q., Umar, A., Sodki, E., Amine, A., Xu, L. N., Gui, Y. G., et al. (2018c). Fabrication and characterization of highly sensitive and selective sensors based on porous NiO nanodisks. *Sens. Actuator. B Chem.* 259, 604–615. doi: 10.1016/j.snb.2017.12.050

Zhou, Q., Xu, L. N., Umar, A., Chen, W. G., and Kumar, R. (2018d). Pt nanoparticles decorated SnO2 nanoneedles for efficient CO gas sensing applications. *Sensor. Actuator. B Chem.* 256, 656–664. doi: 10.1016/j.snb.2017.09.206

Zhou, Q., Zeng, W., Chen, W. G., Xu, L. N., Kumar, R., and Umar, A. (2019). High sensitive and low-concentration sulfur dioxide (SO2) gas sensor application of heterostructure NiO-ZnO nanodisks. *Sens. Actuator. B Chem.* 298, 126870. doi: 10.1016/j.snb.2019.126870

Zhu, L., Li, Y. Q., and Zeng, W. (2017). Enhanced ethanol sensing and mechanism of Cr-doped ZnO nanorods: experimental and computational study. *Ceram. Int.* 43, 14873–14879. doi: 10.1016/j.ceramint.2017.08.003

Zhu, L., Li, Y. Q., and Zeng, W. (2018a). Hydrothermal synthesis of hierarchical flower-like ZnO nanostructure and its enhanced ethanol gas-sensing properties. *Appl. Surf. Sci.* 427, 281–287. doi: 10.1016/j.apsusc.2017.08.229

Zhu, L., Zeng, W., Ye, H., and Li, Y. Q. (2018b). Volatile organic compound sensing based on coral rock-like ZnO. *Mater. Res. Bull.* 100, 259–264. doi: 10.1016/j.materresbull.2017.12.043

**Conflict of Interest:** GQ, QP, DZ, SW, and BY were employed by the company Electric Power Science Research Institute of Yunnan Power Grid Co., Ltd.